THE ASTROPHYSICAL JOURNAL, 437:351–360, 1994 December 10


# X-RAY–INDUCED IONIZATION IN THE WINDS OF NEAR–MAIN-SEQUENCE O AND B STARS

J. J. MACFARLANE,[1,2] D. H. COHEN,[1] AND P. WANG[2]
*Received 1994 April 14; accepted 1994 June 13*

## ABSTRACT

We investigate the effects of X-rays on the ionization state of stellar winds for O and early-B stars along the main sequence. In our investigation, detailed statistical equilibrium, radiative transfer, and atomic physics models are used to compute ionization distributions for H, He, C, N, O, and Si. X-rays are modeled as a spatially distributed source within the wind, with parameters constrained by *ROSAT* and *Einstein* observations. Our results indicate that the ionization balance in the winds of stars with spectral type B0 V and later is significantly altered by the X-ray radiation field. Unlike the case of denser O star winds, where the X-rays tend to *perturb* the level of ionization, the ionization state of the bulk wind of early-B stars can be significantly increased by soft X-rays. We examine in detail the case of $\tau$ Sco (B0 V), which has been well-studied at UV and X-ray wavelengths. Comparisons are made between calculated ionization fractions and those deduced from UV observations. In addition, we address the sensitivity of our results to the X-ray source characteristics, the wind temperature, and the photospheric EUV flux. Our results suggest the possibility that for early-B stars X-rays play a critical role in both influencing the radiation line driving force, as well as ionizing and heating the wind all the way down to the top of the photosphere.

*Subject headings:* radiative transfer — stars: early-type — stars: mass loss — X-rays: stars

## 1. INTRODUCTION

X-ray satellite observations have shown that essentially all early-type stars (spectral class O through early-B) are strong sources of X-ray emission (Harnden et al. 1979; Long & White 1980; Cassinelli et al. 1981). Spectral data from O stars indicate their X-rays are emitted from hot plasmas with characteristic temperatures of about 3–10 $\times$ $10^6$ K, with X-ray luminosities being $\sim 10^{-7} L_{\rm bol}$ (Cassinelli & Swank 1983; Chlebowski et al. 1989). Moderate-resolution X-ray spectra ($\lambda/\Delta\lambda \approx 10$ at $h\nu = 1$ keV) of $\zeta$ Pup (O4 If) measured with the Broad Band X-Ray Telescope (BBXRT) show line emission from highly ionized Mg (Corcoran et al. 1992), clearly indicating thermalized emission from a high-temperature plasma. *ROSAT* X-ray observations of near–main-sequence B stars (Cassinelli et al. 1994a) suggest that $L_x/L_{\rm bol}$ decreases from $10^{-7}$ to $10^{-9}$ between spectral types B1 and B3. B star spectra are often found to be much softer than O stars, with characteristic plasma temperatures being about 1–4 $\times$ $10^6$ K. In addition, recent higher resolution spectra ($\lambda/\Delta\lambda \approx$ 200–400) of $\epsilon$ CMa (B2 II) obtained by the *Extreme Ultraviolet Explorer* (*EUVE*) satellite show emission from several Fe lines with ionization stages ranging from Fe IX through Fe XVI, which is attributed to emission originating from plasma regions with temperatures distributed in a range from 1 to 3 million degrees (Cassinelli et al. 1994b).

Several explanations have been proposed for the source of X-ray emission from O and B stars. Cassinelli & Olson (1979) suggested that a coronal X-ray source could account for the presence of "superionization" stages (e.g., O VI and N V) which are observed in their high-speed winds. This hypothesis, however, appears to be at odds with the fact that X-ray spectral observations do not show significant absorption from an overlying cool wind. Alternatively, Chlebowski (1989) suggested that the X-rays originate far from the star due to the interaction of the stellar wind with circumstellar matter. This appears unlikely though as MacFarlane et al. (1993) have shown that such source is *not* consistent with the observed O VI P Cygni profile of $\zeta$ Pup. The reason is because X-rays cannot penetrate back through the wind to produce sufficient amounts of O VI near the base of the wind. The Chlebowski hypothesis may also be at odds with BBXRT data for $\zeta$ Pup (Corcoran et al. 1992), which shows hints of oxygen K-shell absorption from the overlying wind. Chen & White (1991) have argued that X-rays with energies $\gtrsim$2 keV could be produced as UV photons are scattered by relativistic electrons which have been accelerated in wind shocks. Such a source, however, does not appear to be required to explain the X-ray data since a thermalized high-temperature (i.e., line-emitting) source appears to be fully capable of accounting for the observed spectra from early-type stars.

Lucy & White (1980) and Lucy (1982) proposed that the X-rays are produced by strong shocks propagating through their winds. Indeed, detailed investigations of the formation and growth of shocks which arise due to line-driven instabilities (Owocki, Castor, & Rybicki 1988; Owocki 1991) suggest that strong shocks begin forming in the wind at $r \lesssim 1.5R_*$. A shock-produced X-ray origin can readily explain the lack of significant oxygen K-shell absorption in X-ray spectra because of the reduced column density of overlying cool wind between the source and the observer. Nonmonotonic velocity distributions in the wind can also explain the black absorption troughs observed in UV P Cygni profiles (Lucy 1982, 1983). It has also been shown that the X-ray emission from early B stars, which have relatively low density winds, can be explained by shocks propagating through their winds (MacFarlane & Cassinelli 1989).

Although X-rays are ubiquitous to early-type stars, their effect on the ionization state of winds remains to a large degree unexplored. Early studies (e.g., Cassinelli & Olson 1979; Olson

[1] Department of Astronomy, University of Wisconsin, 475 North Charter, Madison, WI 53706.
[2] Fusion Technology Institute, University of Wisconsin, 1500 Johnson Drive, Madison, WI 53706.

& Castor 1981; Odegard & Cassinelli 1982) estimated the effects of Auger ionization on O and B supergiant stellar winds using very approximate models for ionization, radiative transfer, and X-ray emission. More detailed studies of the ionization state of hot star winds have been carried out by Klein & Castor (1978), Pauldrach (1987), and Drew (1989). Pauldrach performed wind ionization calculations using very detailed atomic models and demonstrated the important role excited states of atoms play in enhancing the degree of ionization in the wind. He also suggested this effect is so strong that the O VI in the wind of $\zeta$ Pup could be produced without X-ray photoionization. Drew, on the other hand, used less detailed atomic models, but calculated the temperature distribution in the wind. Her results predict that heavy-element line cooling should lead to a considerable reduction in the wind temperature—to as low as $0.3T_{\rm eff}$ at $10R_*$—and because of this argued that it is likely that O VI is generated by X-rays. Drew also suggests that localized regions of compression brought on by shocks can explain why models seriously underestimate the abundance of Si IV in O star winds, as well as alter H$\alpha$ emissivities (Drew 1990). However, neither Pauldrach nor Drew included the effects of X-rays in their ionization balance calculations.

Recently, MacFarlane et al. (1993) studied the effects of X-rays on the ionization balance of $\zeta$ Pup using detailed X-ray emission and atomic models. They used an X-ray emission source which was distributed throughout the wind to mimic the emission from multiple shocks. Their results showed that a significant source of X-rays from $\zeta$ Pup must originate in the low-velocity portion of the wind in order to explain its observed O VI P Cygni profile. They also showed that dielectronic recombination has a significant effect on reducing the abundance of high ionization stages, and that the O VI profile of $\zeta$ Pup is produced by, and in fact can be a useful diagnostic for, the X-ray source.

In this paper, we present results describing how the X-ray sources of O and early B near–main-sequence stars affect the ionization state of their winds. Stars near the main sequence were chosen because: (1) their mass-loss rates (and wind densities) decrease sharply from O4 stars ($\dot{M} \gtrsim 10^{-6}\ M_\odot\ {\rm yr}^{-1}$) to early B stars ($\dot{M} \lesssim 10^{-8}\ M_\odot\ {\rm yr}^{-1}$); and (2) the X-ray characteristics of several near–main-sequence stars (O9.5 through B3) have recently been measured with *ROSAT* (Cassinelli et al. 1994a). In our investigation, we use detailed ionization balance, radiative transfer, and atomic physics models to predict the ionization distributions. The X-ray source characteristics—such as the plasma temperature and flux—are constrained by *ROSAT* and *Einstein* IPC (Imaging Proportional Counter) observations. Results are shown describing how the X-rays dramatically alter the ionization state of stars with lower density winds (i.e., the early B stars). We also discuss the sensitivity of the calculated ionization distributions to uncertainties in the X-ray source characteristics, photospheric extreme ultraviolet (EUV) flux, and wind temperature.

## 2. MODEL DESCRIPTION

In this section, we briefly describe the major features of our wind ionization model. Additional details can be found elsewhere (MacFarlane et al. 1993). Table 1 lists some selected parameters of the stars modeled in this investigation. These stars were selected on the following basis: (1) they all lie near the main sequence; (2) their X-ray spectra have been measured by either *ROSAT* or *Einstein*; (3) they are roughly equally spaced in $T_{\rm eff}$; (4) they have been observed at UV wavelengths by either *Copernicus* or *IUE* (*International Ultraviolet Explorer*); and (5) they provide a wide range of wind densities (mass-loss rates). Listed for each star are the spectral type, radius, distance, effective temperature, and surface gravity deduced from observations. The last two columns correspond to the model atmosphere values of $T_{\rm eff}$ and log $g$ used to provide the photospheric flux at the base of the wind in our calculations (see below).

The wind is assumed to be spherically symmetric, with a velocity which increases monotonically with radius:

$$v(r) = v_0 + (v_\infty - v_0)\left(1 - \frac{R_*}{r}\right)^\beta , \qquad (1)$$

where $v_\infty$ is the terminal (i.e., maximum) velocity, $R_*$ is the stellar radius, and $v_0$ is the velocity at the base of the wind. For all calculations discussed in this paper, $\beta = 0.8$ and $v_0 = 0.01 v_\infty$ were assumed. The wind density distribution, $\rho(r)$, was set up by assuming a spatially uniform mass flux: $\rho(r) = \dot{M}/(4\pi r^2 v)$. The temperature distributions in the wind were based on the results of Drew (1989). For the cooler stars in our sample ($T_{\rm eff} < 30{,}000$ K), extrapolations based on Drew's results were used. The sensitivity of our results to the wind temperature is discussed in § 3.1.

Atomic level populations were calculated at each point in the wind by solving multilevel statistical equilibrium equations self-consistently with the radiation field. The following processes were considered: photoionization and photoexcitation; collisional excitation, de-excitation, ionization, and recombination; spontaneous and stimulated emission; and radiative, stimulated, and dielectronic recombination. Energy levels and oscillator strengths were determined from Hartree-Fock calculations (Wang 1991). LS coupling was used to model the angular momentum coupling between electrons. Allowed transitions between pairs of excited states were collisionally coupled, while all excited states of an ion were collisionally coupled with their ground state. Photoexcitation rates were computed in the Sobolev approximation (Castor 1970). Photoionization out of all subshells was considered, with bound-free

TABLE 1

SELECTED STELLAR PARAMETERS

| Star | HD Number | Spectral Type | Radius ($R_\odot$) | Distance (pc) | $T_{\rm eff}$ (K) (observed) | log $g$ (cgs) (observed) | $T_{\rm eff}$ (K) (model) | log $g$ (cgs) (model) |
|---|---|---|---|---|---|---|---|---|
| 9 Sgr ..... | 164794 | O4 V ((f)) | 16 | 1600 | 46,400 | 3.91 | 45,000 | 4.00 |
| 15 Mon ..... | 47839 | O7 V ((f)) | 10 | 700 | 40,100 | 3.89 | 40,000 | 4.00 |
| $\mu$ Col ..... | 38666 | O9.5 V | 6 | 700 | 34,500 | 4.06 | 35,000 | 4.00 |
| $\tau$ Sco ..... | 149438 | B0 V | 6.7 | 170 | 31,500 | 4.15 | 30,000 | 4.00 |
| $\lambda$ Sco ..... | 158926 | B1.5 IV | 7.8 | 110 | 24,000 | 3.73 | 25,000 | 4.00 |
| $\alpha$ Pav ..... | 193924 | B2.5 V | 5.2 | 57 | 19,000 | 3.87 | 20,000 | 4.00 |

cross sections for each subshell determined from Hartree-Fock calculations. In the case of K-shell photoionization, it was assumed the autoionization states immediately depopulate to the ground state of the next higher ionization stage (e.g., O IV goes directly to O VI). Thus, autoionization states were not explicitly included in the model. Dielectronic recombination rate coefficients were taken from Nussbaumer & Storey (1983). The model wind consisted of H, He, C, N, O, and Si in proportions given by the cosmic abundances of Allen (1973). A total of approximately 200 atomic levels distributed over 36 ionization stages was considered.

The radiation field included three emission sources: photospheric radiation, diffuse radiation from the "cool" component of the wind, and radiation from the hot X-ray–emitting plasma. The photospheric radiation field was taken from the model atmospheres of Mihalas (1972). Since the values of the effective temperature, $T_{\rm eff}$, and gravity, $g$, deduced from observations do not fall exactly on the $T_{\rm eff}$-log $g$ grid of computed model atmospheres, we simply chose to use the model fluxes computed for nearby grid points. These values are listed in the last two columns of Table 1. The Mihalas models are non–LTE atmospheres which do not include heavy-element line blanketing. Kurucz (1979) LTE line blanketed model atmospheres often predict a significantly lower EUV flux, and the sensitivity of calculated wind ionization to uncertainties in the photospheric EUV flux for O stars has been studied by Drew (1989). We also address this issue below.

Diffuse radiation is included by solving the second-order form of the radiative transfer equation along a grid of impact parameters (see, e.g., Mihalas, Kunasz, & Hummer 1975; Mihalas 1978). The photospheric flux is input at the base of the wind, while the space-dependent X-ray emissivity is included in the source function. The X-ray source was assumed to have a spatially uniform temperature, with the emissivity given by

$$\eta_\nu^x(r) = \frac{1}{4\pi}\,\Gamma(r)\Lambda_\nu(T_x)\,, \qquad (2)$$

where $\Gamma(r)$ is the volume derivative of the X-ray emission measure, $\mathrm{EM}_x(\equiv \int dV n_e^x n_{\rm H}^x)$, $T_x$ is the temperature of the X-ray source, and $\Lambda_\nu(T_x)$ is the frequency-dependent cooling parameter computed using XSPEC (Raymond & Smith 1977). The differential emission measure was specified by $\Gamma(r) = Cn_w^2(r)$, where $n_w(r)$ is the cool wind density and $C$ is a constant constrained by the observed X-ray flux.

Table 2 shows the X-ray and wind parameters adopted for this study. X-ray parameters for $\mu$ Col, $\tau$ Sco, $\lambda$ Sco, and $\alpha$ Pav are based on the analysis of recent *ROSAT* observations while those for 9 Sgr and 15 Mon are based on *Einstein* IPC observations. Note that for $\tau$ Sco, only the X-ray parameters derived from the single-temperature (1-T) fit to the data are listed in Table 2. We also performed calculations for $\tau$ Sco using 2-T X-ray models. The parameters for these models are defined in § 3.1. Also note that $T_x$ for $\alpha$ Pav is assumed, as there were insufficient counts in the *ROSAT* observations to determine the X-ray temperature accurately. Also shown are the mass-loss rates and terminal velocities adopted for this study. The mass-loss rates for 9 Sgr and 15 Mon are based on H$\alpha$ observations, while that of $\tau$ Sco is taken from the analysis of UV observations. The terminal velocities for 9 Sgr, 15 Mon, $\mu$ Col, and $\tau$ Sco are based on UV observations. The remainder of the values for $\dot{M}$ and $v_\infty$ are based on either extrapolations of the $\dot{M} - L_{\rm bol}$ relation of Howarth & Prinja (1989) or theoretical models (Friend & Abbott 1986; Pauldrach, Puls, & Kudritzsky 1986) as described in Cassinelli et al. (1994a).

TABLE 2

ADOPTED X-RAY AND WIND PARAMETERS

| Star | $L_x$ ($10^{30}$ ergs s$^{-1}$) | $T_x$ ($10^6$ K) | $\dot{M}$ ($10^{-8}$ $M_\odot$ yr$^{-1}$) | $v_\infty$ (km s$^{-1}$) |
|---|---|---|---|---|
| 9 Sgr | 580[a] | 10[a] | 240[d] | 2950[g] |
| 15 Mon | 230[b] | 5.8[b] | 50[d] | 2300[g] |
| $\mu$ Col | 76[c] | 2.3[c] | 3.2[e] | 2100[h] |
| $\tau$ Sco | 58[c] | 9.3[c] | 0.7[f] | 2000[f] |
| $\lambda$ Sco | 2.7[c] | 1.5[c] | 0.63[e] | 1400[i] |
| $\alpha$ Pav | 0.039[c] | 1.5[c] | 0.031[e] | 1300[i] |

[a] Cassinelli et al. 1981.
[b] Chlebowski et al. 1989.
[c] Cassinelli et al. 1994a.
[d] Lamers & Leitherer 1993.
[e] Howarth & Prinja 1989.
[f] Lamers & Rogerson 1978.
[g] Groenewegen & Lamers 1989.
[h] Olson & Castor 1981.
[i] Theory.

## 3. RESULTS

Below we describe results which show the effects of X-rays on the ionization state of the stars listed in Tables 1 and 2. We first describe in detail the results for $\tau$ Sco. In a sense, this star represents a rather extreme case for X-ray–induced ionization because it has a very large X-ray flux for a star with such a weak, low-density wind. In particular, we examine the influence of X-ray spectral characteristics on the wind ionization. Second, we study the effect of X-rays as a function of spectral type, and discuss the relative effects of photospheric and X-ray ionization. Finally, we compare our results for $\tau$ Sco with wind ionization fractions deduced from UV observations.

### 3.1. *Calculated Ionization Distributions for $\tau$ Sco*

To illustrate the dramatic effect X-rays can have on the ionization distributions in the winds of early B stars, let us first simply compare the results from two calculations for $\tau$ Sco: one in which X-rays were included, the other in which they were ignored. In the former case, the frequency dependence of the X-ray spectrum is prescribed by a two-temperature XSPEC model with $T_{X,1} = 1.3 \times 10^6$ K and $T_{X,2} = 8 \times 10^6$ K, which are based on those derived from *ROSAT* observations (Cassinelli et al. 1994a). The emission measures of the two components, however, were adjusted to produce reasonably good agreement with the *ROSAT* data (described in more detail below). The ratio of the two components was $\mathrm{EM}_{X,1}/\mathrm{EM}_{X,2} = 0.25$.

The calculated ionization fractions, $q$, for He, C, N, and O are shown in Figure 1 as a function of the scaled velocity ($v/v_\infty$). For each atomic element, the results for the case in which X-rays were neglected are shown in the upper portion of the plot. For He (*upper left*), it is seen that in the case without X-rays, He II (*curve with open triangles*) is predicted to be the dominant ionization stage, while $q$(He III) $\lesssim 2 \times 10^{-2}$. Very little He I is expected ($\lesssim 10^{-6}$). On the other hand, when X-rays are included, He III is predicted to be the dominant ionization stage, while $q$(He II) falls to $\sim 10^{-2}$ to $10^{-1}$. The reason for this is that relatively little flux is emitted from the *photosphere* at photon energies above the He II photoioniza-

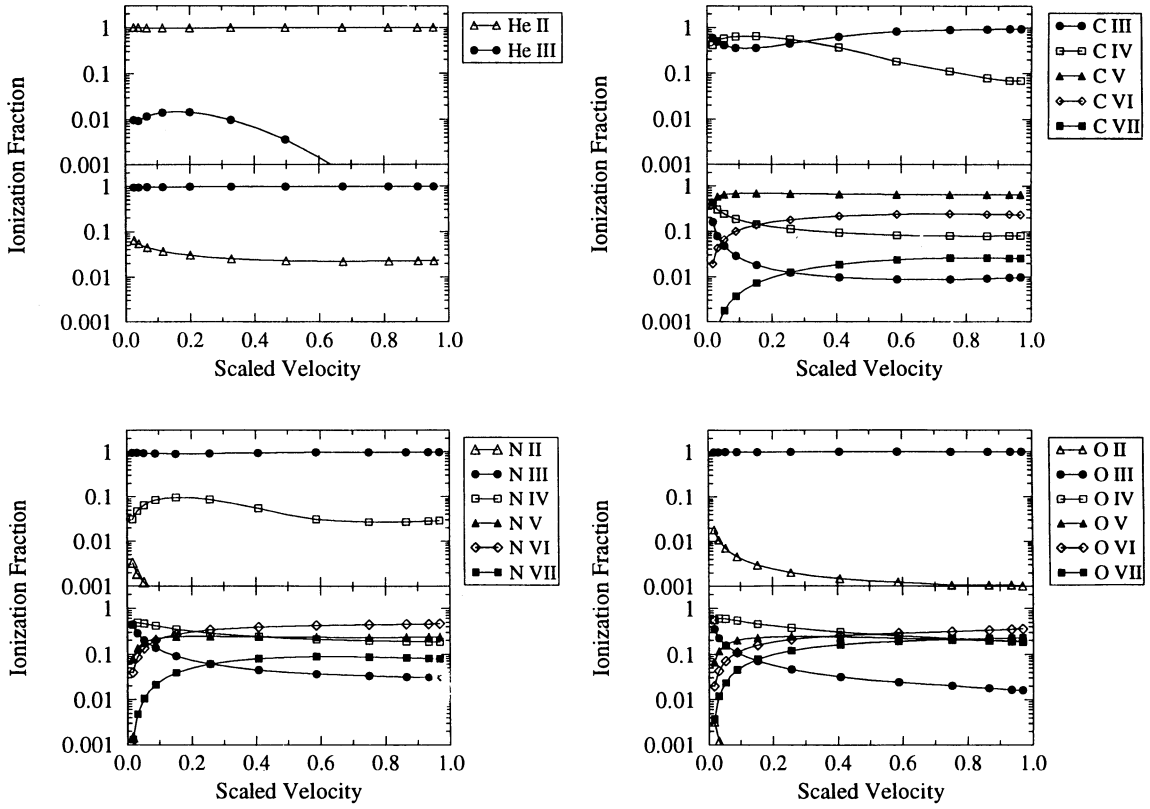


FIG. 1.—Calculated ionization fractions in the wind of $\tau$ Sco as a function of scaled velocity $[v(r)/v_\infty]$ for ions of He, C, N, and O. For each element, the lower panel represents from calculations in which X-rays were included, while the upper panel corresponds to calculations in which they were neglected. Note the significant shift to higher degrees of ionization when X-rays are included.

tion threshold at 54.4 eV. When X-rays are introduced in the calculation, there is considerably greater flux in the soft X-ray/EUV region of the spectrum, which comes predominantly from the low-temperature component of the X-ray model. Indeed, observational support for such an enhancement in the He ionization comes from recent *EUVE* observations of $\epsilon$ CMa (B2 II), which shows He II Ly$\alpha$($\lambda$ = 304 Å) strongly in emission (Cassinelli et al. 1994b). This emission results from He III—which becomes "overpopulated" due to X-rays—recombining into the $n = 2$ state of He II, which subsequently decays to the ground state.

Results from C, N, and O show similar effects. In the absence of X-rays, relatively low ionization stages—C III–IV, N III, and O III (*filled circles*)—are predicted to be the dominant species. Photoionization does not proceed efficiently to higher ionization stages because of the dearth of photospheric photons above the thresholds of these ions (N III: 47.4 eV; C III: 47.9 eV; O III: 54.9 eV; C IV: 64.5 eV). Again, however, when X-rays are included in the calculations the ionization shifts significantly to higher stages. For instance, C V is predicted to be the dominant ionization stage of carbon. This result is qualitatively consistent with *Copernicus* observations (Lamers & Rogerson 1978; hereafter LR) in that C III and C IV are likely to be trace species ($q \sim 10^{-3}$ to $10^{-2}$ for $\dot{M} = 7 \times 10^{-9}\ M_\odot\ \mathrm{yr}^{-1}$). Nitrogen and oxygen are also predicted in our calculations to be spread over several high-ionization stages. For example, N IV–VII and O IV–VII all have ionization fractions $\gtrsim 10^{-1}$. Ionization to the highest stages occurs by K-shell photoabsorption, which requires photons with energies of several hundred eV or more. This portion of the soft X-ray spectrum is reasonably well-constrained from *ROSAT* observations.

It is also interesting to note that high-ionization stages can be formed even down to the base of the wind, which corresponds to an areal mass depth ($= \int_{R_*}^{\infty} \rho\, dr$) of $1 \times 10^{-3}$ g cm$^{-2}$ and an electon scattering optical depth of $3 \times 10^{-4}$ in the $\tau$ Sco calculations. This suggests that the X-rays could significantly alter the ionization distribution, and perhaps even the temperature distribution in the upper portion of the photosphere. If this is true, it may become necessary to include the effects of an external X-ray source when trying to deduce the properties of early B star photospheres from model atmosphere calculations.

We next address the sensitivity of the calculated wind ionization distributions to the X-ray model, wind temperature, and photospheric flux shortward of the H Lyman edge ($\lambda < 912$ Å). Figure 2 shows the C III ionization distribution from five different calculations. In case A a single-temperature X-ray model was used with $T_x = 10^7$ K, which is approximately equal to the value determined from fitting the *ROSAT* spectrum (Cassinelli et al. 1994a). In this case the C III ionization fraction is substantially higher—about a factor of 20 at $v = 0.5v_\infty$—than in the previously described 2-T X-ray model (labeled curve C in Fig. 2). This shift to lower ionization for case A occurs because of the reduced flux in the X-ray model at $h\nu \approx 50$–200 eV; i.e., at photon energies just above the photoionization thresholds of C III and C IV. Case B represents results from a 2-T X-ray

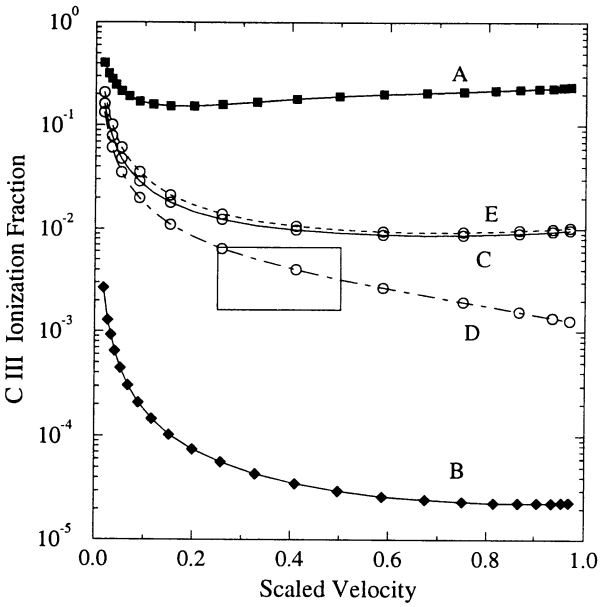


FIG. 2.—Sensitivity of calculated C III ionization fraction to X-ray model parameters, wind temperature, and photospheric EUV flux. X-ray model A corresponds to a 1-T ($T_x = 10^7$ K) spectrum; X-ray model B coresponds to a 2-T spectrum ($T_{x,1} = 1.3 \times 10^6$ K, $T_{x,2} = 8 \times 10^6$ K, $EM_{x,1}/EM_{x,2} = 3$); X-ray model C corresponds to a 2-T spectrum with a weaker soft component ($T_{x,1} = 1.3 \times 10^6$ K, $T_{x,2} = 8 \times 10^6$ K, $EM_{x,1}/EM_{x,2} = 0.25$). Calculations D and E are identical to case C, but with $T_{wind} = 30{,}000$ K (case D), and no photosphere EUV flux (case E). The open box represents results derived from the analysis of *Copernicus* UV observations (LR).

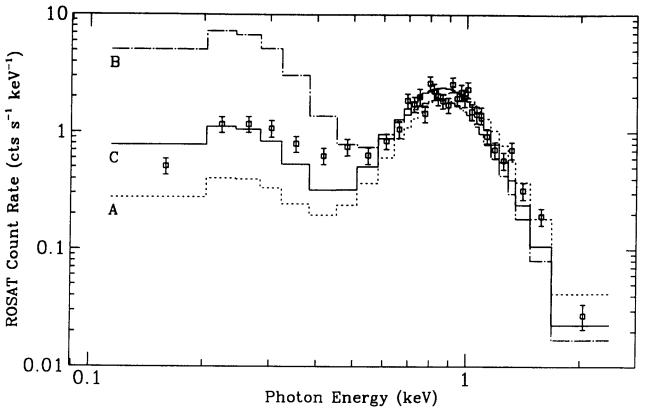


FIG. 3.—Comparison of calculated X-ray spectra with *ROSAT* spectrum (*boxes with error bars*) for $\tau$ Sco. The model spectra were obtained by feeding the higher resolution computed spectra through the *ROSAT* instrumental response. The calculated spectra correspond to X-ray models A, B, and C described in Fig. 2.

model with $T_{x,1} = 1.3 \times 10^6$ K and $T_{x,2} = 8 \times 10^6$ K (i.e., the same as case C), but in this case the ratio of the emission measures of the two components was taken to be that determined from fits to the *ROSAT* data: $EM_{x,1}/EM_{x,2} = 3$ (Cassinelli et al. 1994a). The C III fraction in this calculation is more than two orders of magnitude lower than that of case C. These calculations show the critical role soft X-ray/EUV radiation emitted by the lower temperature component(s) of the X-ray emitting plasma plays in affecting the ionization balance.

Also shown in Figure 2 are results from calculations which used the same X-ray emission model as case C, but with either a different wind temperature or photospheric flux. Cases D and E are identical to case C except for the following. In case D the wind was assumed to be isothermal with $T_{wind} = 30{,}000$ K (as opposed to using a distribution based on Drew 1989). In case E the photospheric flux at $\lambda < 912$ Å was completely neglected. Case D shows that by increasing the wind temperature, the C III fraction is reduced as the carbon shifts to higher ionization. This occurs because both the radiative and dielectronic recombination rates decrease with increasing temperature (Nussbaumer & Storey 1983). For case E, it is seen that photospheric radiation with $\lambda < 912$ Å has little effect on the C III fraction. This is because the photoionization rate between the ground states of C III and C IV is dominated by the X-ray field. It is important to note, however, that not all ions behave this way. For instance, the He I fraction increases by two to three orders of magnitude when the photospheric flux shortward of 912 Å is neglected, which is due to its photoionization edge being at lower energy (24.6 eV).

The calculated fluxes from cases A, B, and C are compared with the observed *ROSAT* spectrum for $\tau$ Sco in Figure 3. This was done by taking the computed flux at the outer boundary of the computational grid ($R_{max} = 30R_*$), and then correcting for ISM attenuation and the distance to the Earth. The resultant fluxes were then fed through the *ROSAT* instrumental response to make a direct comparison with the observed spectrum (*boxes with error bars*). In each case the total X-ray emission measure was adjusted so that the model spectrum was in good agreement with the observed spectra at $h\nu \gtrsim 0.6$ keV. At these energies attenuation by the overlying wind is expected to be negligible. At lower energies there are significant differences between the models. When the low-temperature component is neglected (case A), the calculated flux is a factor of 2–3 lower than the observed flux. This need for emission from a lower temperature component was pointed out in Cassinelli et al. (1994a). However, when using the emission measure ratio previously derived from the 2-T fit to the *ROSAT* data (case B), we find the calculated flux at $h\nu \lesssim 0.3$ keV is about an order of magnitude too high. The reason for this apparent discrepancy is that the previous 2-T *ROSAT* fit was determined using a very rudimentary absorption model. The total absorbing column density (wind plus ISM) was an adjustable parameter, with the value determined from a $\chi^2$ minimization of the fit to the X-ray data. In addition, the opacities used in the data reduction package were neutral element opacities, which of course overestimate the absorption due to He in the wind (see Fig. 1). Thus, the higher EM for the low-temperature component in this case was significantly attenuated, thereby resulting in a good fit to the observed spectrum. When using a 2-T model with a reduced emission measure for the low-temperature component (case C), the calculated spectrum agrees reasonably well with the observed spectrum. The largest differences for this case appear at 0.4–0.5 keV. It may be that the distribution of temperatures in the X-ray emitting regions are better represented by a continuous (e.g., power-law) emission measure distribution (Cohen et al. 1994).

It is interesting to note that the model which produces the best agreement with the X-ray spectrum also produces best agreement with the ionization fraction deduced from UV observations with $\dot{M} = 7 \times 10^{-9}$ $M_\odot$ yr$^{-1}$ (LR). The "observed" fractions at $v = 0.25v_\infty$ and $0.5v_\infty$ are indicated by the box in Figure 2, where a factor of 2 uncertainty was arbi-

trarily placed on the derived C III fraction. Although the C III fraction computed for case C is a factor of a few too large, it is considerably closer than the cases in which the X-ray models were based on previous 1-T and 2-T fits to the *ROSAT* observations. It is also in much better agreement than the model in which X-rays were neglected entirely (see Fig. 1), where without X-rays, C III is predicted to be the most abundant stage of carbon. We therefore conclude that X-rays can play a major role in altering the "bulk" ionization balance in the wind of $\tau$ Sco. That is, the X-rays are not simply a perturbation which results in the formation of trace amounts of high-ionization stages (such as in the case of O VI for $\zeta$ Pup), but actually have the capability of altering the ionization of the bulk of the wind.

### 3.2. *Dependence of Wind Ionization on Spectral Type*

Ionization balance calculations were performed for our six main-sequence stars using the X-ray and wind parameters listed in Table 2. The exception to this is $\tau$ Sco, where the 2-T X-ray model (case C) was used. For each star, the temperature of the X-ray–emitting plasma remained fixed, while the total emission measured was adjusted until agreement with the observed X-ray luminosity was achived. In addition, a series of calculations was performed in which X-rays were neglected in order to examine the impact X-rays have on the wind ionization state.

Figure 4 shows the calculated ionization fractions at $v = 0.5v_\infty$ for He II–III, C III–V, N III–V, and O III–VI as a function of the stellar effective temperature. The solid diamonds represent results from calculations in which X-rays were included, while the open circles represent those in which X-rays were neglected. For each ion, a general trend emerges. The influence of X-rays increases with decreasing stellar effective temperature. For example, for stars with $T_{\rm eff} \gtrsim 35{,}000$ K (i.e., the O stars) He III, C V, N IV–V, and O IV are predicted to be the dominant ionization stages in both the X-ray and no X-ray cases. For these stars, only for the highest ionization stages—O VI and, in the case of $\mu$ Col, N V and O V—does the ionization fraction change significantly. However, the differences between the X-ray and no X-ray results are significantly greater for the B stars. For instance, He II and C III are the most abundant ions in the B star calculations when X-rays are neglected, while the ionization fractions are extremely small for He III, C V, and for $\lambda$ Sco and $\alpha$ Pav, C IV. When X-rays are included, these higher ionization stages attain significantly higher populations. Similar effects are seen for nitrogen and oxygen, where N III and O II–III are predicted to be the dominant stages in the absence of X-rays. With X-rays, the N IV and O IV fractions are $\gtrsim 10^{-1}$. In fact for $\tau$ Sco, which again has an extraordinarily high X-ray flux, N IV–VI and O IV–VII (i.e., up through He-like nitrogen and oxygen) all have ionization fractions greater than $10^{-1}$ in calculations where X-rays are included. This shift to higher ionization for B stars is augmented by the fact that the densities of their winds are significantly lower than those of O stars.

Another interesting result which is seen in Figure 4 is that for B stars the X-rays are capable of producing a very broad distribution in the ionization of each element. For instance, in the $\lambda$ Sco and $\alpha$ Pav calculations without X-rays we find that six CNO ions—C II–III, N II–III, and O II–III—have ionization fractions with $q \gtrsim 10^{-3}$. When X-rays are included this number rises to 13 as C IV–V, N IV–VI, and O IV–V also attain fractions with $q \gtrsim 10^{-3}$. One potentially important implication of this is that the radiation force on the wind will be changed. It could potentially increase as the number of lines available for accelerating the wind increases due to the increasing number of "abundant" ionization stages. On the other hand, the radiation force might actually decrease since the lines from the highest ionization stages tend to reside at wavelengths where the photospheric flux is much lower.

The reason X-rays play an increasingly important role for stars with lower effective temperatures can be understood by examining Figure 5. Here, the photospheric flux at the top of the photosphere (as specified by Mihalas 1972 non–LTE model atmospheres and indicated by the dotted curves) is compared with the X-ray flux (*solid curves*) for 9 Sgr (O4), $\tau$ Sco (B0), and $\alpha$ Pav (B2.5). The X-ray flux is constrained by the observed flux, and adjusted by $(D/R_*)^2$. Note that the ordinates in Figure 5 vary over approximately 15 orders of magnitude. Also shown at the top of the figure are the approximate ionization thresholds for several ions. For 9 Sgr, it is seen that the photospheric flux dominates out to relatively high photon energies ($\sim$80–90 eV). At the other extreme, the X-ray flux for $\alpha$ Pav exceeds the photospheric flux all the way down to 30–40 eV, which is below the ionization potentials of nearly all the ions shown. For $\tau$ Sco, the transition from a photospheric-dominated to X-ray–dominated spectrum occurs at approximately 50 eV. Thus, for most ions photoionization rates should be expected to be strongly dependent on the characteristics of the X-ray source for main-sequence stars with spectral type B0 and later.

The mean charge state from the calculations described above is shown for each element in Figure 6 as a function of stellar effective temperature. The mean charge is given by

$$\langle q(E) \rangle = \sum_{j=0}^{Z} j q_E^{j+} , \qquad (3)$$

where $Z$ is the atomic number of element $E$. (Note that $He^{2+}$ = He III.) Again it is seen that for the hottest stars (9 Sgr and 15 Mon), the X-rays make only a slight perturbation on the charge state of the bulk of the wind. However, for the B stars, and to some extent $\mu$ Col, the mean ionization state for the bulk wind can shift substantially. The most extreme case is $\tau$ Sco, which has a high X-ray luminosity while having, presumably, a low mass-loss rate. For the B stars, shifts of one to two full ionization stages can be seen.

Our results also suggest that the X-rays may be capable of significantly *heating* the winds of early B stars. That is, if the X-rays are capable of altering the ionization state of the bulk wind, one would also expect they could cause significant heating. This effect was not included in our calculations as a fixed temperature distribution was assumed.

### 3.3. *Comparison between Model Results and UV Observations*

As pointed out by Groenewegen and Lamers (1991), serious discrepancies exist between theory and observation when it comes to predicting the ionization state of hot star winds. Comparisons between ionization fractions deduced from UV observations of O stars and calculations reported by Pauldrach (1987) and Drew (1989) showed discrepancies ranging up to factors of $10^2$–$10^3$ in $\dot{M}q$ (the product of mass-loss rate times ionization fraction). They argued that both calcuations tended to predict too much ionization as Si IV tended to be underestimated and C IV overestimated for late O stars. For earlier O

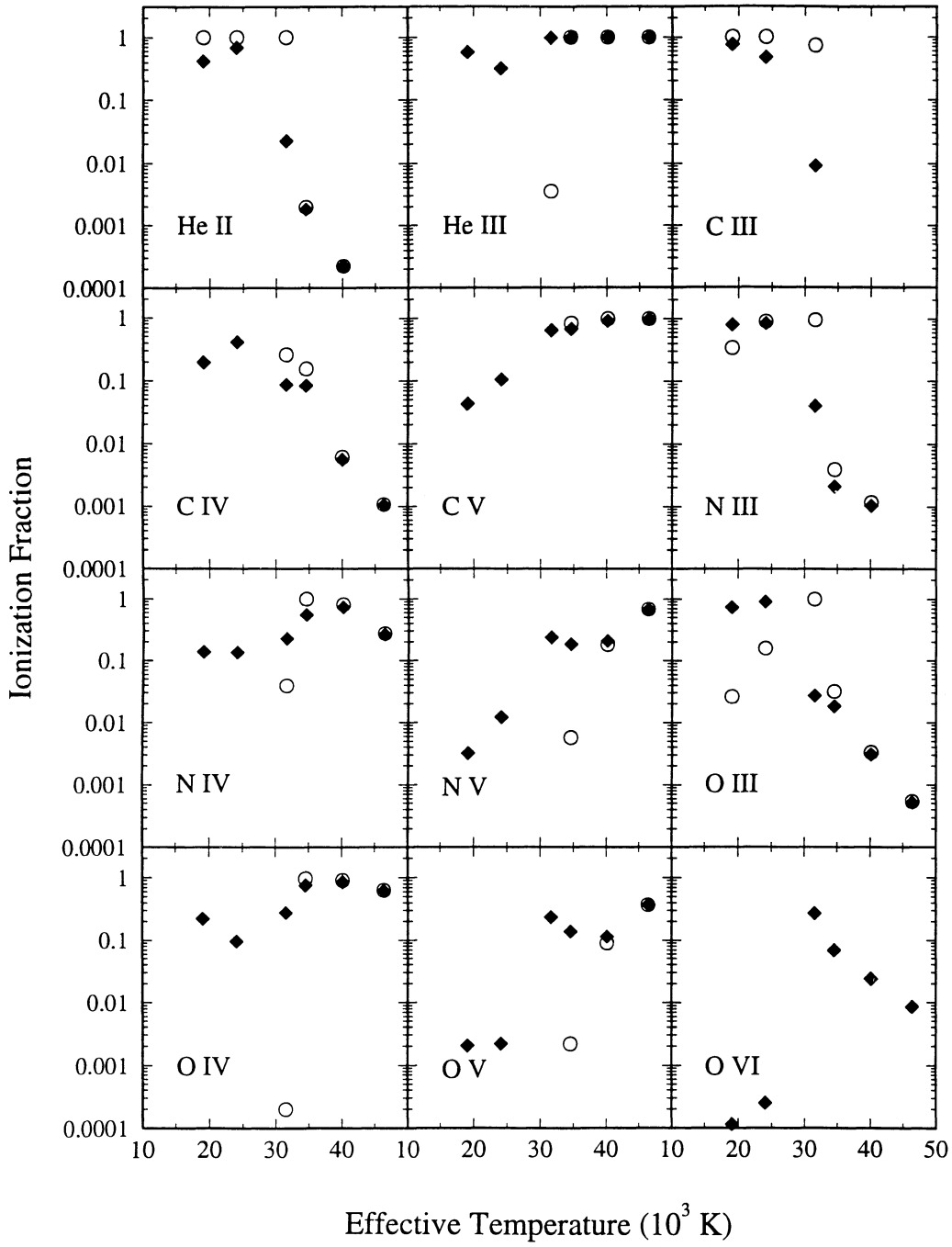


FIG. 4.—Ionization fractions calculated at $v = 0.5v_\infty$ as a function of stellar effective temperature for the stars listed in Table 2. The solid diamonds represent results from calculations in which X-rays were included, the open circles correspond to those in which X-rays were neglected.

stars (O5–O7) N V was overestimated, but was underestimated for later O stars. The latter can be explained by the fact that the Pauldrach and Drew calculations did not include X-rays.

We find similar trends in our results, which we will illustrate by comparing results for $\tau$ Sco with ionization fractions derived from UV observations. Figure 7 shows our calculated ionization distributions for wind lines observed by *Copernicus* (LR) and *IUE* (Prinja 1989). These lines are Si IV ($\lambda\lambda$1393.8, 1402.8), N III ($\lambda\lambda$989.8, 991.6), C III ($\lambda$977.0), C IV ($\lambda\lambda$1548.2, 1550.8), N V ($\lambda\lambda$1238.8, 1242.8), and O VI ($\lambda\lambda$1031.9, 1037.6). Results are shown in order of increasing ionization potential (*top to bottom*). The ionization fractions are plotted in terms of $\dot{M}q$, which can be obtained from the analysis of UV line profiles. Although the Prinja results are plotted at $w = 0.5$, it is worthwhile noting that his derived terminal velocity was 1200 km s$^{-1}$, while that of LR was 2000 km s$^{-1}$. The solid thicker curves correspond to the X-ray model which produced the best agreement with the *ROSAT* data (see Fig. 3). The curves from

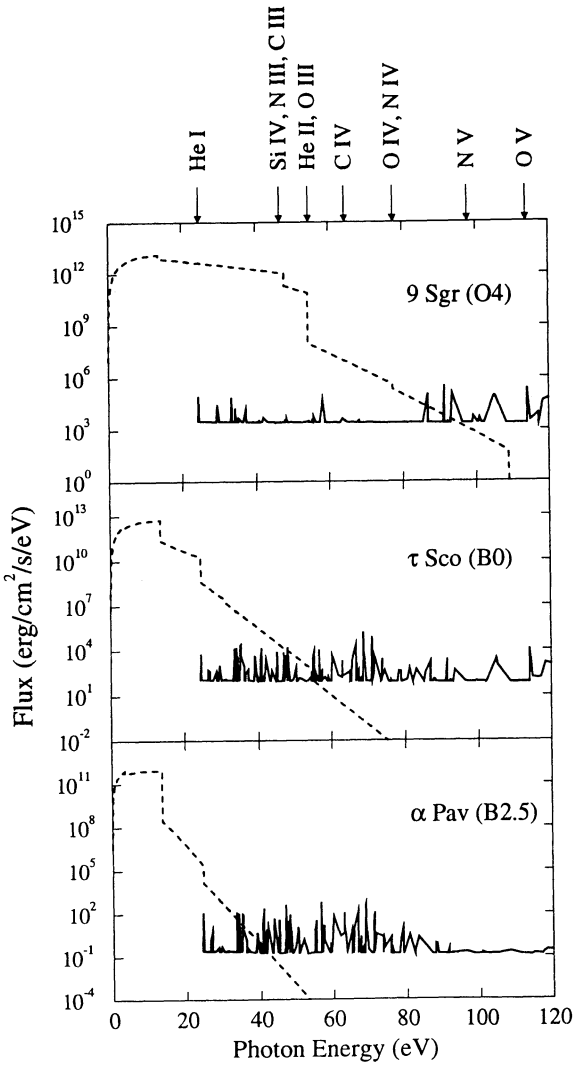


FIG. 5.—Model photospheric and X-ray spectra used in calculations for 9 Sgr, τ Sco, and α Pav. Fluxes are normalized to $r = R_*$. Note that the photon energy at which the X-ray flux exceeds the photospheric flux decreases for stars with lower effective temperatures. The photoionization energies for several important ions are shown at the top.

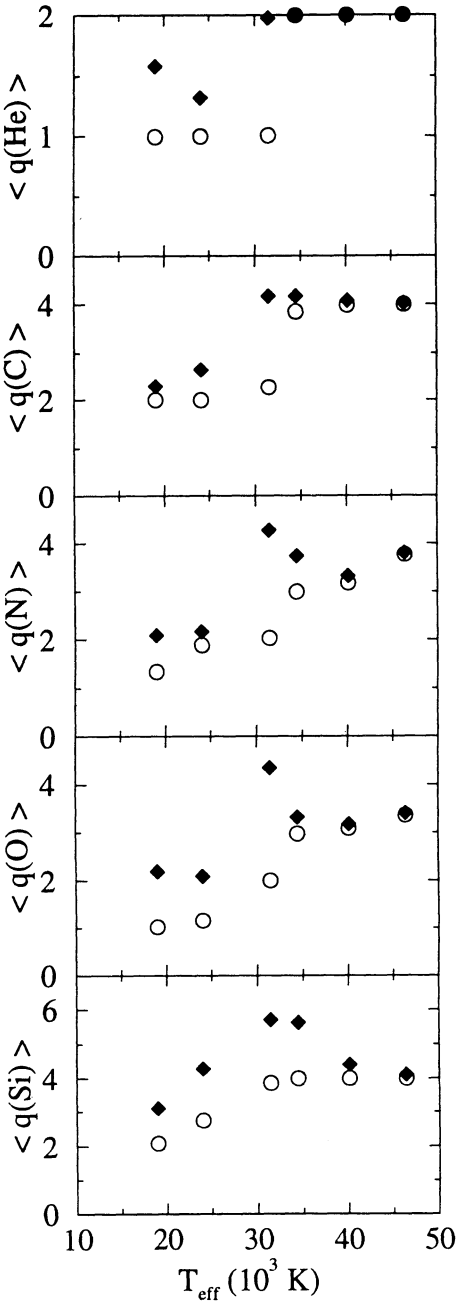


FIG. 6.—Average charge state of He, C, N, O, and Si calculated at $v = 0.5v_\infty$ as a function of stellar effective temperature. Symbol definitions are the same as those in Fig. 4.

the other models are shown to illustrate the sensitivity of the calculated ionization fractions to the soft X-ray/EUV flux.

Figure 7 shows that our calculations tend to overestimate the N V and O VI ionization fractions by approximately one order of magnitude regardless of which X-ray model is used. The C IV fraction is also about one order of magnitude too high in the model which best agrees with the *ROSAT* data. In contrast, the calculated C III, N III, and Si IV ionization fractions are generally within a factor of a few of the observed values. Thus a clear trend emerges in which the ionization fractions of ions with the highest ionization potentials are overestimated in the calculations.

Although this conclusion was reached in previous comparisons between theory and observations, it is important to note an important difference between the previous calculations and ours. In our calculations for τ Sco, X-rays are the main source of radiation which produces the more highly ionized species; in particular, C IV, N V, and O VI. This source of radiation is reasonably well-constrained down to photon energies ≈0.1–0.2 keV by *ROSAT* observations. In contrast, the primary radiation source in the O star calculations of Pauldrach and Drew was photospheric EUV radiation, which is a part of the spectrum which is not at all constrained from observations. Thus, it is somewhat more difficult for us to attribute differences between theory and observation entirely to uncertainties in the radiation field.

An alternative explanation for overestimating $\dot{M}q$ for the more highly ionized species (N V and O VI) is the uncertainty in

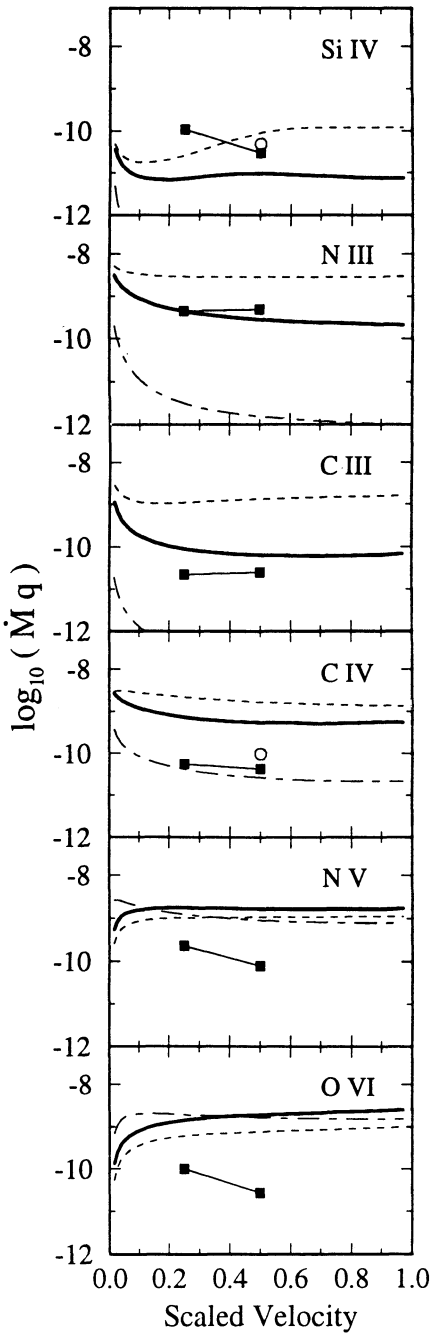


FIG. 7.—Comparison of calculated ionized fractions (multiplied by the mass-loss rate) with those deduced from UV observations of $\tau$ Sco. Filled squares at $v = 0.25$ and $0.5v_\infty$ are from Lamers & Rogerson (1978); open circles are from Prinja (1989). The calculated distributions correspond to X-ray models C (*thick solid curve*), A (*dashed curve*), and B (*dash-dotted curve*) shown in Fig. 2 and described in § 3.1.

the wind density. However, attempts to decrease the wind ionization for $\tau$ Sco by simply increasing the mass-loss rate quickly fail as the C III fraction increases rapidly with $\dot{M}$. Indeed, $\dot{M}q$ for C III and C IV are already overestimated in our calculations with $\dot{M} = 7 \times 10^{-9}\ M_\odot\ \mathrm{yr}^{-1}$.

Perhaps a more likely reason for persisting differences between theory and observation is that all wind ionization models to date fail to account for any "structure" in the wind that should arise from radiatively driven instabilities and shocks, as has been suggested by Drew (1989). The observed X-ray emission from O and B stars is commonly attributed to shock-heated regions in the wind. If this is true, one should expect the density distribution in the wind to deviate significantly from the "steady state" case, where $\rho = \dot{M}/4\pi r^2 v$. Radiation-hydrodynamics simulations of the growth of radiately driven instabilities predict fluctuations of up to three orders of magnitude (Owocki et al. 1988). In such a structured wind one would expect the lower ionization stages (e.g., C III, Si IV) to dominate in the high-density regions, while higher ionization stages should reside in the lower density regions. We intend to investigate the ionization state of structured winds in a future study.

## 4. CONCLUSIONS

From our investigation, it is concluded that X-rays are likely to be the primary source of ionizing radiation in early B star winds at photon energies $\gtrsim 50$ eV; i.e., near the ionization thresholds of many of the ions which are observed as wind lines in UV spectra. Because of this, and because of their lower density, X-rays can significantly alter the bulk ionization state of B star winds. This is very different from the case of denser O star winds, where X-rays tend to produce merely a perturbation on the overall ionization state. In the case of O stars, trace—but observable—amounts of highly ionized species (e.g., O VI and N V) are produced.

Our calculated ionization distributions for B stars were found to be very sensitive to the soft X-ray/EUV emission from our model X-ray source. This was exemplified in calculations using 1-T and 2-T X-ray models, where it was shown that the C III fraction decreased by one to three orders of magnitude when a low-temperature X-ray component was included. Comparisons with ionization fractions derived from UV observations of $\tau$ Sco showed our calculated ionization fractions for N V and O VI to be somewhat high, while those for the relatively low ionization stages of Si IV, N III, and C III were in better agreement with observation. It is argued that the discrepancies between theory and observation are likely due to structure in OB star winds which results from radiatively driven instabilities and shocks.

The dramatic impact X-rays have on B star winds could have several important ramifications. First, it was found that X-rays tend to "broaden" the ionization distribution so that more ions become highly populated. For example, the number of CNO ions with ionization fractions $\gtrsim 10^{-3}$ approximately doubled when X-rays were included in the calculations. This change in the bulk ionization state of the wind might significantly impact the radiation line-driving force. Second, because the X-rays are capable of changing the bulk ionization state of B star winds, it seems possible that they could significantly heat the winds as well. We also find that significant amounts of highly ionized species can be produced all the way down to the base of the wind in our calculations, suggesting that both the ionization distribution, and perhaps even the temperature, at the top of the photosphere could be significantly impacted by the X-rays. These possibilities will be the subject of future investigations.

The authors thank J. P. Cassinelli and J. E. Drew for many stimulating discussions on this topic. This work has been supported in part by NASA grant NAGW-2210.

REFERENCES


Allen, C. W. 1973, Astrophysical Quantities (3d ed.; London, Athlone)
Cassinelli, J. P., et al. 1994b, ApJ, to be submitted
Cassinelli, J. P., Cohen, D. C., MacFarlane, J. J., Sanders, W. T., & Welsh, B. Y. 1994a, ApJ, in press
Cassinelli, J. P., & Olson, G. L. 1979, ApJ, 229, 304
Cassinelli, J. P., & Swank, J. H. 1983, ApJ, 271, 681
Cassinelli, J. P., Waldron, W. L., Sanders, W. T., Harnden, F. R., Rosner, R., & Vaiana, G. S. 1981, ApJ, 250, 677
Castor, J. I. 1970, MNRAS, 149, 111
Chen, W., & White, R. L. 1991, ApJ, 366, 512
Chlebowski, T. 1989, ApJ, 342, 1091
Chlebowski, T., Harnden, F. R., & Sciortino, S. 1989, ApJ, 341, 427
Cohen, D. H., et al. 1994, in preparation
Corcoran, M. F. 1992, ApJ, 412, 792
Drew, J. E. 1989, ApJ, 71, 267
———. 1990, ApJ, 357, 573
Friend, D. B., & Abbott, D. C. 1986, ApJ, 311, 701
Groenewegen, M. A. T., & Lamers, H. J. G. L. M. 1989, A&A, 79, 359
———. 1991, A&A, 243, 429
Harnden, F. R., et al. 1979, ApJ, 234, L51
Howarth, I. D., & Prinja, R. K. 1989, ApJS, 69, 527
Klein, R. I., & Castor, J. I. 1978, ApJ, 220, 902
Kurucz, R. L. 1979, ApJS, 40, 1
Lamers, H. J. G. L. M., & Leitherer, C. 1993, ApJ, 412, 771
Lamers, H. J. G. L. M., & Rogerson, J. B. 1978, A&A, 66, 417 (LR)
Long, K. S., & White, R. L. 1980, ApJ, 239, L65
Lucy, L. B. 1982, ApJ, 255, 286
———. 1983, ApJ, 274, 372
Lucy, L. B., & White, R. L. 1980, ApJ, 241, 300
MacFarlane, J. J., & Cassinelli, J. P. 1989, ApJ, 347, 1090
MacFarlane, J. J., Waldron, W. L., Corcoran, M. F., Wolff, M. J., Wang, P., & Cassinelli, J. P. 1993, ApJ, 419, 813
Mihalas, D. 1972, NCAR Tech. Note, STR-76
———. 1978, Stellar Atmospheres (2d ed.; New York: Freeman)
Mihalas, D., Kunasz, P. B., & Hummer, D. C. 1975, ApJ, 202, 465
Nussbaumer, H., & Storey, P. J. 1983, A&A, 126, 75
Odegaard, N., & Cassinelli, J. P. 1982, ApJ, 256, 568
Olson, G. L., & Castor, J. I. 1981, ApJ, 244, 179
Owocki, S. P. 1991, in Stellar Atmospheres: Beyond Classical Models, ed. I. Hubeny & L. Crivellari, NATO Advanced Study Workshop (Dordrecht: Kruwer)
Owocki, S. P., Castor, J. I., & Rybicki, G. B. 1988, ApJ, 235, 914
Pauldrach, A. 1987, A&A, 183, 295
Pauldrach, A. W. A., Puls, J., & Kudritzsky, R. P. 1986, A&A, 164, 86
Prinja, R. K. 1989, MNRAS, 241, 721
Raymond, J. C., & Smith, B. W. 1977, ApJS, 35, 419
Wang, P. 1991, Ph.D. dissertation, Univ. Wisconsin, Madison